Physica B 625 (2022) 413536

Contents lists available at ScienceDirect

Physica B: Physics of Condensed Matter

journal homepage: www.elsevier.com/locate/physb

Morphology controlled $(CH_3NH_3)_3Bi_2Cl_9$ thin film for lead free perovskite solar cell

Paramesh Chandra, Swapan K. Mandal *

Department of Physics, Visva-Bharati, Santiniketan, 731235, India

ARTICLE INFO

Keywords:
Lead-free perovskite
Solar cell
Dip coating
Photovoltaic
Open-circuit voltage
Surface morphology control

ABSTRACT

Traditional perovskite solar cells have made tremendous progress in terms of efficiency in the past few years but the presence of toxic lead (Pb) has restricted their commercialization. We report here a process to fabricate MABiCl perovskite thin film based solar cell. The process shows some intriguing outcomes like uniform surface morphology of the perovskite layer, high open-circuit voltage and good fill-factor. The film shows improved uniform morphology and surface coverage with flakes (dimension 570 nm × 360 nm, thickness ~ 100–200 nm. The solar cell device shows an open-circuit voltage of about 496 mV and a fill factor 0.55. The improved morphology of the perovskite layer with reduced number of defects and charge traps possibly decreases the probability of recombination of photoexcited charge carriers. The result indicates that the process can be a good alternative to prepare lead free perovskite solar cells with improved performance.

1. Introduction

Metal-Organic hybrid perovskite with the general formula of AMX_3 (A = organic group; M = metal ion and X = halide ions) have emerged as a potential material in the field of optoelectronic and photovoltaic applications [1–8]. Hybrid perovskite was first used as a light absorber in solar cells with less than 4% efficiency by Miyasaka's group in 2009 [1]. Since then, a large number of research works were carried out which showed a substantial increase in efficiency in solar energy harvesting. Though at first the efficiency of the perovskite solar cell was considerably low and stability was poor, in the year 2012, some breakthrough reports [9,10] changed the course of Perovskite Solar Cell (PSC) research. Lead-based hybrid perovskite recently achieved its highest efficiency of 25.5% [11]. $CH_3NH_3PbX_3$ is also used in other applications due to its high absorption coefficient and high carrier mobility. Although $CH_3NH_3PbX_3$ perovskites are desired materials for various applications, low stability, high sensitivity towards moisture and the presence of highly toxic lead (Pb) restrict their commercialization [12]. So, extensive investigations are being conducted by various researchers to replace Pb in the perovskite without sacrificing efficiency and achieving higher stability.

Some possible strategies to make the solar cell more efficient are replacement of Pb metal ion, optimizing the surface morphology of the thin films and find the best possible architecture for the device fabrication. The goal of the work is to find a suitable metal ion to replace Pb in the perovskite and exploring the possibilities to improve the process of device fabrication to gain more control over the morphology of the film and to further boost the efficiency and stability of the solar cell. It has been hypothesized that the defect-tolerant perovskite electronic structure could be replicated in materials consisting of a heavy metal cation with a stable pair of valence s electrons. This is why we have considered bismuth (Bi^{3+}) (electron configuration [Xe] ($4f^{14}$ 5 d^{10} $6s^2$ $6p^3$) which forms a stable 3+ oxidation state, leading to stable $6s^2$ valence electrons and giving rise the possibility of replicating the Pb^{2+} (electron configuration [Xe] ($4f^{14}$ 5 d^{10} $6s^2$ $6p^2$) ion-based perovskite electronic structure [13]. Bi^{3+} being a heavy metal cation, band dispersion due to spin-orbit coupling is expected. In addition, Bi^{3+} similar to Pb^{2+} is also a largely polarizable cation and possesses a high Born effective charge leading to high dielectric constants that are important for increased screening of charged defects [13]. Also, the low toxicity of bismuth [14] and lack of exploration of this field makes it a desirable topic for solar cell researchers. Here, we report a simple process to synthesize methylammonium bismuth chloride (MABiCl) perovskite solar cell which gives better morphological control on the films and fabricates a solar cell device with high open-circuit voltage and fill factor.

* Corresponding author.
E-mail address: sk_mandal@hotmail.com (S.K. Mandal).

https://doi.org/10.1016/j.physb.2021.413536
Received 4 April 2021; Received in revised form 7 October 2021; Accepted 3 November 2021
Available online 6 November 2021
0921-4526/© 2021 Elsevier B.V. All rights reserved.

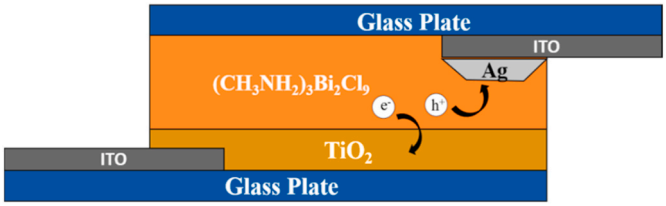

Fig. 1. Schematic diagram of the fabricated solar cell device structure.

2. Experimental details

2.1. Chemicals

The starting materials used for the synthesis of the perovskite material were methylamine, hydrochloric acid, bismuth chloride, anhydrous N, N dimethylformamide (DMF), and for titanium oxide film, titanium-isopropoxide was used. All the chemicals were taken of analytical grade purity and obtained from commercial sources (MERCK and Sigma Aldrich) and used without further purification. For device fabrication indium tin oxide coated glasses (ITO) were used (sheet resistance ~7 Ω/sqm) as the substrate and conductive silver paste of commercial grade were used for making electrical contacts.

2.2. Synthesis of methylammonium bismuth chloride (MABiCl)

CH_3NH_3Cl (MACl) was synthesized by reacting a 1:1 ratio of methylamine (33 wt% in ethanol) and hydrochloric acid (35%) in absolute ethanol in ice at 0 °C for 2 h with stirring at low rpm. A clear solution was obtained which was allowed to evaporate slowly keeping the bath temperature at 50 °C. After that the ethanol was slowly evaporated under continuous stirring at a constant temperature 50 °C in vacuum for 24 h. The evaporation of ethanol resulted in a white precipitate of MACl.

Synthesis of the lead-free Bi-based perovskite $(CH_3NH_3)_3Bi_2Cl_9$ (MABiCl) material as a light absorber was done by mixing 3:2 M ratio CH_3NH_3Cl and Bi_2Cl_3 in DMF. The solution was stirred for half an hour at 50 °C resulting in a white foggy solution. Addition of ethyl alcohol resulted in the formation of a white precipitate. 20 ml ethyl alcohol is added to get a white precipitate. The solution is filtered and dried under a constant temperature 60 °C in vacuum condition to get MABiCl powder.

For the electron transfer layer (ETL), we have used TiO_2 thin film. The TiO_2 solution was prepared adding an excess amount of water with titanium-isopropoxide solution and stirred at 80 °C until a dry white precipitate of TiO_2 is obtained.

2.3. Solar cell fabrication

Planar heterojunction solar cell containing Bi-based perovskite film was fabricated using the following method. Firstly, ITO coated glass substrates (1 cm × 1 cm) were etched with HCl and zinc powder to obtain the required pattern for device fabrication. Then, the ITO glasses were further cleaned with deionized water, ethanol using an ultrasonicator and finally dried in vacuum condition. A compact layer of TiO_2 was deposited using a dip-coating method. The earlier prepared TiO_2 powder is mixed with ethanol and the substrate is dipped in the solution. The substrate is dipped and dried sequentially. The film was dried using hot airflow. After the successful deposition of the TiO_2 film, the substrate was annealed at 450 °C for 1 h TiO_2 coated substrate was then dipped (10 times) in MABiCl mixed with ethanol solution till we get a perovskite film with a desired thickness. The whole system of layers is kept at 100 °C for 30 min. After that, another ITO glass is attached to the top of the MABiCl layer using the silver paste as the contact layer. The whole device is annealed at 100 °C for 30 min to finalize the process. Care has been taken while making the contacts so that it does not

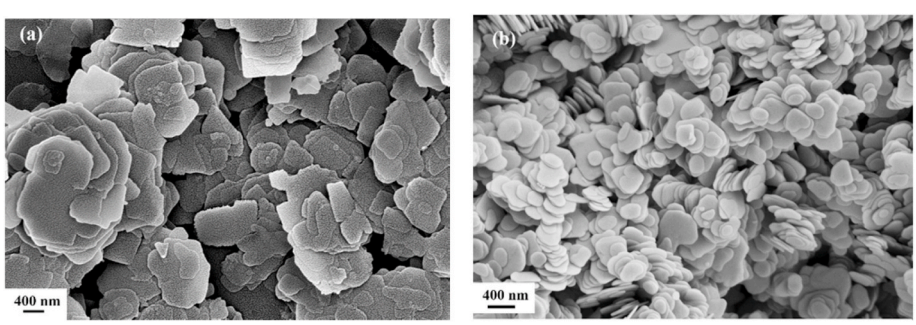

Fig. 2. SEM image of MABiCl perovskite (a) powder sample (b) thin-film sample using the dip-coating method. The powder sample shows irregular and non-uniform growth whereas the thin-film sample shows growth of distinct flakes with large surface coverage and uniformity.

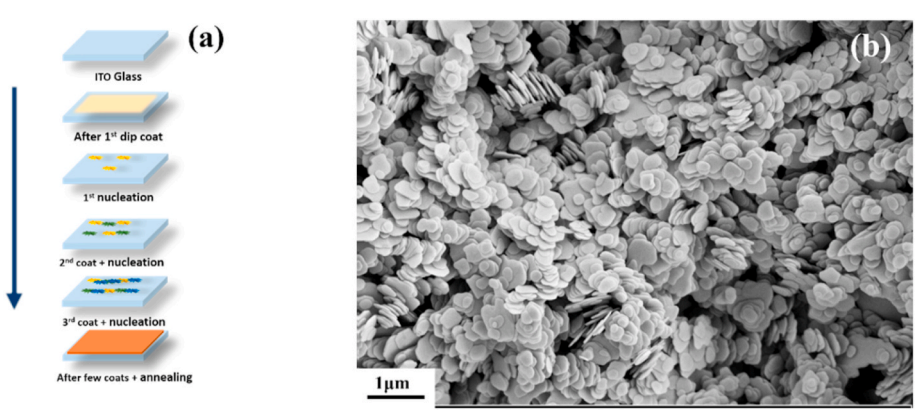

Fig. 3. (a) Sequential deposition technique of the MABiCl perovskite film. (b) SEM morphology of MABiCl film on ITO substrate.

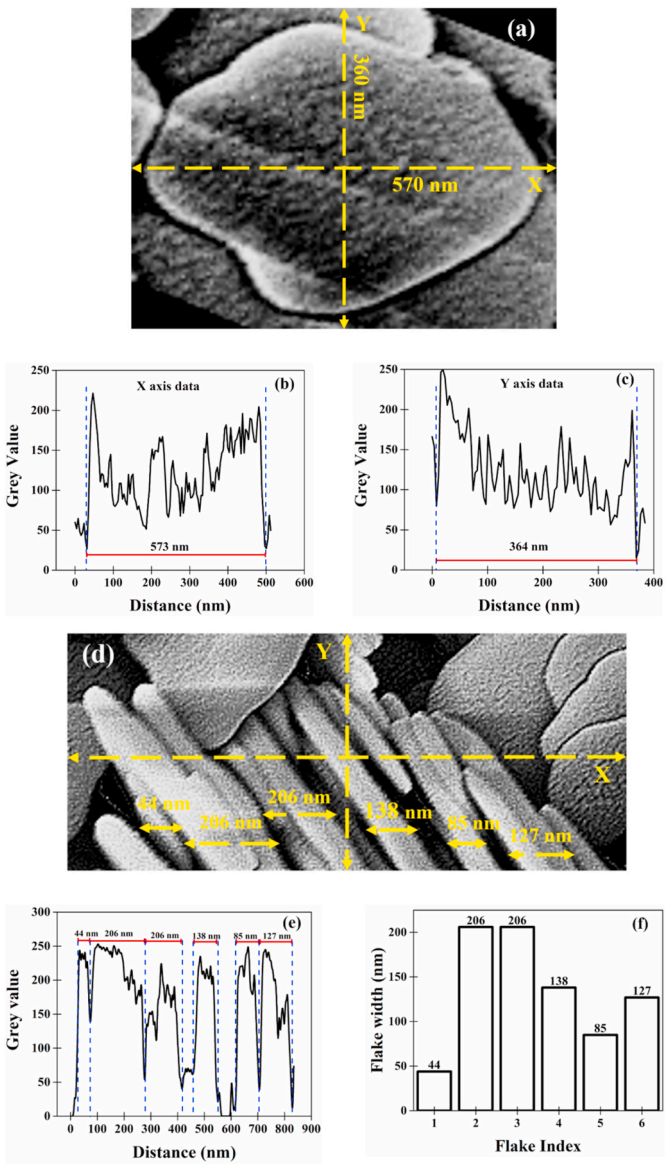

Fig. 4. **(a)** Flat surface of a clear flake with length along X-axis is 570 nm and along Y-axis is 360 nm, **(b)** plot of the grey value of the pixels and distance of the pixel from initial along X-axis for the flat surface **(c)** plot of the grey value of the pixels and distance of the pixel from initial point along Y-axis for the flat surface. **(d)** cluster of flakes having visibly distinct flakes with thickness 44 nm, 206 nm, 206 nm, 138 nm, 85 nm and 127 nm respectively from left. **(e)** plot of the grey value of the pixels and distance of the pixel from initial along X axis for the perpendicular surfaces of the flakes and **(f)** the thickness of each flake vs. flake index.

penetrate the thin layers of MABiCl (thickness ~ 400 nm) and TiO_2 to touch the ITO glass of the opposite side to prevent the problem of short-circuiting the device. A schematic diagram of the fabricated solar cell device is shown in Fig. 1.

2.4. Instruments and characterizations

Scanning electron microscopy (SEM ZEISS GEMINI SEM 450) was used to study the morphology of the films. Optical properties were measured with Beckman Coulter DU720 UV–Vis spectrometer. The photovoltaic performance was characterized under the illumination of the vertically stacked LED lamps using Keithley 6514 electrometer.

3. Results and discussion

The microstructures of the MABiCl samples are shown in Fig. 2a-b. In Fig. 2a, SEM image of the powder sample of MABiCl is shown which shows an irregular distribution of the MABiCl flakes but on the other hand, the thin film sample deposited on ITO substrate shows a regular distribution of the flakes (disc-shaped) with uniform size distribution as shown in Fig. 2b.

This morphology plays a significant role in the transportation of excited electrons and holes to the electrodes. A better morphology causes an increase in crystallinity and decrease of defects which in turn stimulates less recombination and proves to be important in the enhancement of performance. The powder sample without any treatment tends to form big and irregular flakes but the thin film shows growth of regular small flakes with higher surface coverage. During the deposition process, a constant flow of hot air is maintained. The smaller particle size (dimensions of typical flake: length 570 nm and breadth 360 nm) of thin film sample may be caused due to the airflow as the sample reaches its supersaturation faster than that of the powder sample. And the uniformity and good surface coverage may also be the outcome of a slow and steady coating procedure. In general, the precipitation of a solution into a film involves two conditions: nucleation and crystal growth. Nucleation will be formed when the solution reaches supersaturation. Thus, slow evaporation indicates a low degree of precursor supersaturation. This will cause crystal growth with a small number of particles and with aggregation on the surface as shown in Fig. 2a. The flow of air may be one of the approaches to control the state of precursor superposition as the results are consistent with previous report [15]. Controlled sequential dipping and coating of the film perhaps provide suitable condition to obtain a uniform film with high density and coverage as schematically shown in Fig. 3a. The procedure clearly showed the formation of a uniform film with a high density of flakes as revealed by the SEM image given in Fig. 3b.

We have further analyzed the SEM images with ImageJ software [16] and took a profile (grey value of the pixels where 0 signifies black and 255 signifies white) the most visibly clear flake and tried to fit the profile for a few other flakes with the clear one. Fig. 4a shows the flat surface of a clear flake used for profile plotting. In Fig. 4b and c, the grey value of the pixels and the distance of the pixel from the initial point for the X-axis and Y-axis are plotted accordingly. Considering a steep descent of the grey value to be an edge, we have calculated the length (along X-axis) and width (along Y-axis) of the flake which are 570 nm and 360 nm respectively. From Fig. 4a, it can be said that that the flake tends to form an ellipsoidal shape with major axis a = 570 nm and minor axis b = 360 nm. To calculate the thickness of the flakes, we have selected a cluster of visibly distinct flakes present in the cluster as shown in Fig. 4d. The profile plot of the grey value shows consecutive minima for each edge as depicted in Fig. 4e. The distance between two consecutive minima is considered to be the thickness of the flakes. We found the thickness of the flakes to vary between 100 and 200 nm. The flake width and flake index are also plotted in Fig. 4f for convenience. The thickness of the film is measured to be less than 300 nm (approx.).

The optical absorption of perovskite thin film and that of TiO_2 film are shown in Fig. 5a and b respectively. The direct optical band gap of the semiconducting nanostructure was determined using Taucs' plot by plotting $(\alpha h\nu)^2$ vs. $h\nu$. The calculated bandgap of the perovskite thin film is found to be 2.58 eV which is very close to the reported value of 2.51 eV [17]. The bandgap of the TiO_2 film is 4.35 eV where the bulk bandgap is between 3 and 3.2 eV. The bandgap of TiO_2 tends to change with film preparation procedure [18,19].

Fig. 6a shows the X-ray diffraction data of the perovskite film. The data has been compared with the Crystallographic Information File (CIF) as shown in Fig. 6b [20]. The XRD pattern showed a high degree of crystallinity of the film. Though the crystal structure of the material belongs to the centrosymmetric orthorhombic Pnma space group [20], we have found some additional small peaks probably arising out of the

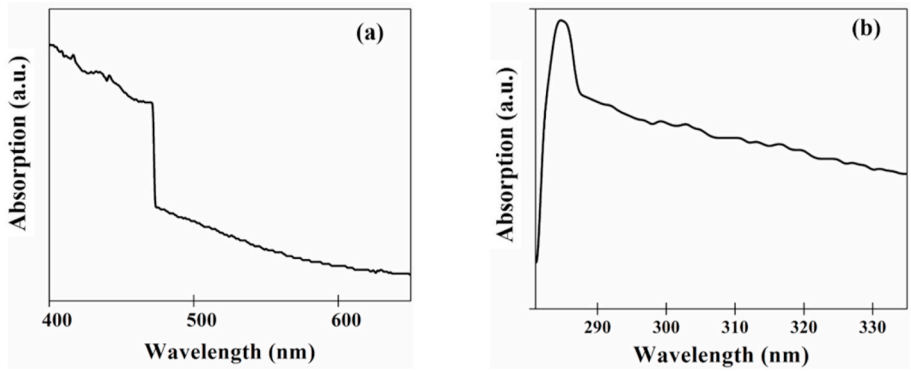

Fig. 5. Optical absorption spectra of (a) MABiCl perovskite film and (b) TiO_2 film used as ETL layer.

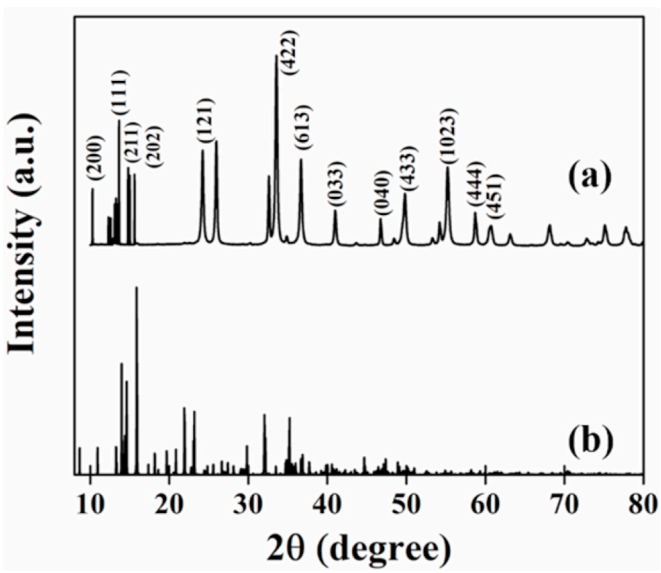

Fig. 6. XRD pattern of (a) the synthesized MABiCl perovskite film and that of (b) provided by the Crystallographic Information File (CIF).

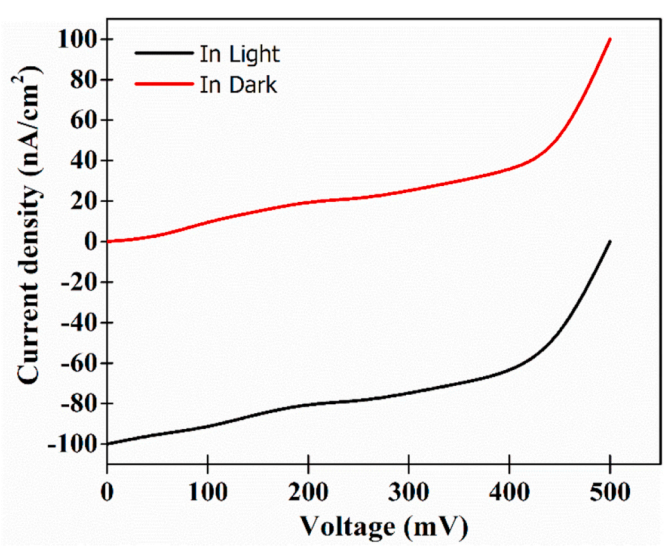

Fig. 7. J-V characteristic curve of the ITO/Meso-TiO_2/$[(CH_3NH_3)_3Bi_2Cl_9]$n/Ag/ITO device.

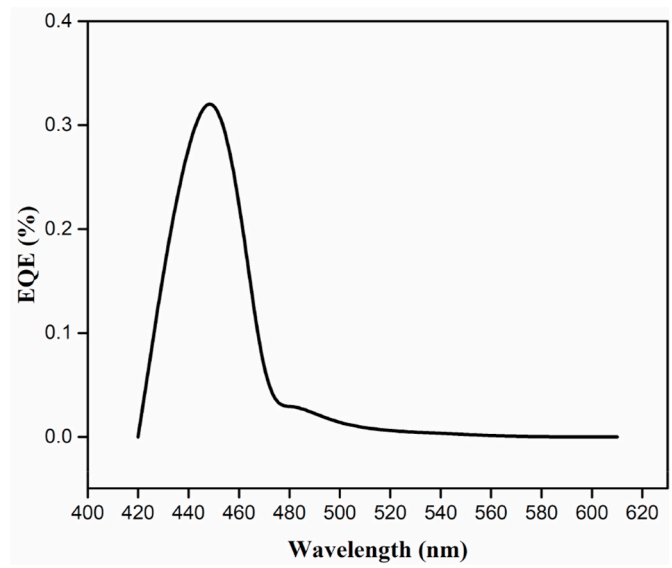

Fig. 8. Measured external quantum efficiency (EQE) of the solar cell device.

Table 1
Comparison of open-circuit voltage of MABiCl based perovskite solar cell devices with other works in contemporary literature.

Light absorber	V_{OC} (mV)	Fill-actor (FF)	Published in year	Ref.
1,6-hexanediammonium bismuth iodide ($HDABiI_5$)	384	0.43	2016	[28]
$(CH_3NH_3)_3Bi_2I_9Cl_X$	40	0.38	2015	[29]
$(CH_3NH_3)_3CuCl_2Br_2$	300	0.32	2016	[30]
$(CH_3NH_3)_3Bi_2I_9$	680	0.33	2015	[29]
$(CH_3NH_3)_3Bi_2I_9$	354	0.454	2016	[31]
1D polymer-$[(CH_3NH_3)_3Bi_2Cl_9]_n$	430	–	2018	[20]
$[(CH_3NH_3)_3Bi_2Cl_9]_n$	**496**	**0.55**	**-**	**This work**

substrate and unreacted Bi.

Current density-voltage (J-V) characteristic was investigated both under dark and illumination using a stacked led light source, having an illumination area of 1 cm^2, and the data were recorded using Keithley 6514 electrometer. The performance of this Pb free PSC with the device architecture (ITO/Meso-TiO_2/$[(CH_3NH_3)_3Bi_2Cl_9]_n$/Ag/ITO) was examined using J-V characteristics under illuminated condition. This kind of hole-conductor-free PSC was first produced by Etgar et al. with efficiency of ~6% for lead based perovskite material [21] which suggested

perovskite can both work as a light absorber and a hole conductor. In some other works using the same architecture and thicker lead-based perovskite layer the efficiency of the device has been found to be improved [21,22]. Meng and his co-workers demonstrated ~10% efficient HTM-free PSC based on a mesoporous TiO_2 scaffold using the two-step solution-deposition method [23–25]. TiO_2 as well as a very thin layer of AlO_x between absorber layer and metal electrode was also used giving rise to an efficiency of 11.1% [25]. These findings clearly indicate that the incorporation of interlayer may help in blocking holes to promote electron transport and thus enhances the efficiency of the device. The recorded J-V characteristic for the fabricated device is shown in Fig. 7. Although the fabricated device showed poor power conversion efficiency (<1%) with the current density in nA range, a decent open-circuit voltage of 496 mV was obtained with considerably good fill-factor (FF) = 0.55. The high open-circuit voltage is assumed to be caused by the non-conventional technique used here to prepare the thin film and hole transport material free device configuration. A higher degree of order present in the MABiCl layer prohibits the generation of defects and charge traps which in turn increases the transport of photoexcited charge carriers to the electrodes of the solar cell and causes lesser chances for recombination of free charge carriers. There are mainly three kind of recombination process to be dominant in perovskite solar cell device. Firstly, monomolecular (i.e., carriers recombine through a recombination centre or commonly known as trap) secondly, bimolecular recombination (i.e., the holes and electron recombination) and lastly the amalgamation of both kind of recombination. Some recent study showed that the recombination mechanism can switch from monomolecular under short circuit conditions to bimolecular under open-circuit conditions [27]. So, the open-circuit voltage is most affected by bimolecular recombination. In case of this device, we have not used any electron or hole blocking layer which can reduce this kind of recombination process to further increase the V_{oc}. The controlled deposition technique we have demonstrated in our work helps to reduce the trap density inside the device which further reduces monomolecular recombination process but it does not help to reduce the bimolecular recombination. Also, we believe that use of better electrode contacts will considerably improve the efficiency of the fabricated solar cell. Fig. 8 further shows the external quantum efficiency (EQE) curve of the device. The band gap of the material is 2.58 eV so the EQE above 500 nm is going down rapidly. Other causes of the low quantum efficiency are firstly the light reflected and absorbed on the outer glass surface of the device, secondly the recombination of electron and holes inside the device and lastly the light sensing range of the device is close to the blue region so there is a little scope for light interaction with the material. Although the peek in the EQE curve near 440 nm can further employed as a light detector of particular frequency.

Furthermore, in Table 1, we have tabulated the fill factor and V_{oc} of some recent works on Bi-based perovskite solar cells. The solar cell presented in this current work gives better V_{OC} than most of them with a comparable good fill factor.

4. Conclusion

In summary, we have prepared a perovskite material MABiCl as the light sensitizer layer to fabricate Pb free perovskite solar cell. The synthesis process adopted here facilitates faster evaporation of the solvent and a sequential deposition of the perovskite film on ITO substrate resulting in better surface coverage, morphology and regular distribution of disc shaped flakes. The solar cell device showed a relatively high open-circuit voltage of 496 mV and good fill factor 0.55. Although solar cell efficiency was found to be low <1%, we believe this could be further improved with use of optimized film thickness, more control on surface morphology and good electrical contacts. Moreover, the absorber layer with a bandgap of 2.58 eV and polymeric structure has the potentiality for use in device applications like photo-detectors, LEDs, batteries and supercapacitors.

Credit authors statement

All the authors contributed equally to the manuscript.

Declaration of competing interest

The authors don't have any potential conflicts of interest include employment, consultancies, stock ownership, honoraria, paid expert testimony, patent applications/registrations, and grants or other funding.

Acknowledgement

The author PC wishes to acknowledge with thanks to DST-PURSE, Visva-Bharati, for providing research fellowship to him during this program.

References

[1] A. Kojima, K. Teshima, Y. Shirai, T. Miyasaka, J. Am. Chem. Soc. 131 (2009) 6050.
[2] J.M. Azpiroz, E. Mosconi, J. Bisquert, F. De Angelis, Energy Environ. Sci. 8 (2015) 2118.
[3] T.Y. Yang, G. Gregori, N. Pellet, M. Grätzel, J. Maier, Angew. Chem. Int. Ed. 54 (2015) 7905.
[4] S.S. Shin, E.J. Yeom, W.S. Yang, S. Hur, M.G. Kim, J. Im, J. Seo, J.H. Noh, S. Il Seok, Science 356 (2017) 167.
[5] Q. Jiang, L. Zhang, H. Wang, X. Yang, J. Meng, H. Liu, Z. Yin, J. Wu, X. Zhang, J. You, Nat. Energy 2 (2017) 16177.
[6] M. Saliba, T. Matsui, K. Domanski, J.Y. Seo, A. Ummadisingu, S.M. Zakeeruddin, J. P. Correa-Baena, W.R. Tress, A. Abate, A. Hagfeldt, M. Grätzel, Science 354 (2016) 206.
[7] M. Saliba, T. Matsui, J.Y. Seo, K. Domanski, J.P. Correa-Baena, M.K. Nazeeruddin, S.M. Zakeeruddin, W. Tress, A. Abate, A. Hagfeldt, M. Grätzel, Energy Environ. Sci. 9 (2016) 1989.
[8] W.S. Yang, J.H. Noh, N.J. Jeon, Y.C. Kim, S. Ryu, J. Seo, S. Il Seok, Science 348 (2015) 1234.
[9] H.S. Kim, C.R. Lee, J.H. Im, K.B. Lee, T. Moehl, A. Marchioro, S.J. Moon, R. Humphry-Baker, J.H. Yum, J.E. Moser, M. Grätzel, N.G. Park, Sci. Rep. 2 (2012) 591.
[10] C.H. Lee, D.R. Kim, I.S. Cho, N. William, Q. Wang, X. Zheng, Sci. Rep. 2 (2012) 1000.
[11] W.S. Yang, B.W. Park, E.H. Jung, N.J. Jeon, Y.C. Kim, D.U. Lee, S.S. Shin, J. Seo, E. K. Kim, J.H. Noh, S. Il Seok, Science 356 (2017) 1376.
[12] F. Giustino, H.J. Snaith, ACS Energy Lett 1 (2016) 1233.
[13] R.E. Brandt, V. Stevanović, D.S. Ginley, T. Buonassisi, MRS Commun 5 (2015) 265.
[14] R. Mohan, Nat. Chem. 2 (2010) 336.
[15] S. Song, M.T. Hörantner, K. Choi, H.J. Snaith, T. Park, J. Mater. Chem. 5 (2017) 3812.
[16] C.T. Rueden, J. Schindelin, M.C. Hiner, B.E. DeZonia, A.E. Walter, E.T. Arena, K. W. Eliceiri, BMC Bioinf. 18 (2017) 529.
[17] T. Kawai, A. Ishii, T. Kitamura, S. Shimanuki, M. Iwata, Y. Ishibashi, J. Phys. Soc. Japan 65 (1996) 1464.
[18] K. Hashimoto, H. Irie, A. Fujishima, Jpn. J. Appl. Phys. 44 (2005) 8269.
[19] N. Serpone, D. Lawless, R. Khairutdinov, J. Phys. Chem. 99 (1995) 16646.
[20] K. Ahmad, S.N. Ansari, K. Natarajan, S.M. Mobin, ACS Appl. Energy Mater. 1 (2018) 2405.
[21] L. Etgar, P. Gao, Z. Xue, Q. Peng, A.K. Chandiran, B. Liu, M.K. Nazeeruddin, M. Gratzel, J. Am. Chem. Soc. 134 (2012) 17396.
[22] W.A. Laban, L. Etgar, Energy Environ. Sci. 6 (2013) 3249.
[23] S. Aharon, B. El Cohen, L. Etgar, J. Phys. Chem. C 118 (2014) 17160.
[24] J. Shi, Y. Luo, H. Wei, J. Luo, J. Dong, S. Lv, J. Xiao, Y. Xu, L. Zhu, X. Xu, ACS Appl. Mater. Interfaces 6 (2014) 9711.
[25] H. Wei, J. Shi, X. Xu, J. Xiao, J. Luo, J. Dong, S. Lv, L. Zhu, H. Wu, D. Li, Y. Luo, Q. Meng, Q. Chen, Phys. Chem. Chem. Phys. 17 (2015) 4937.
[27] S.R. Cowan, J. Wang, J. Yi, Y.-J. Lee, D.C. Olson, J.W.P. Hsu, J. Appl. Phys. 113 (2013) 154504.
[28] D.M. Fabian, S. Ardo, J. Mater. Chem. 4 (2016) 6837.
[29] B.W. Park, B. Philippe, X. Zhang, H. Rensmo, G. Boschloo, E.M.J. Johansson, Adv. Mater. 27 (2015) 6806.
[30] D. Cortecchia, H.A. Dewi, J. Yin, A. Bruno, S. Chen, T. Baikie, P.P. Boix, M. Gra, Inorg. Chem. 55 (2016) 1044.
[31] M. Lyu, J.H. Yun, M. Cai, Y. Jiao, P.V. Bernhardt, M. Zhang, Q. Wang, A. Du, H. Wang, G. Liu, L. Wang, Nano Res 9 (2016) 692.